Copyright Warning & Restrictions

The copyright law of the United States (Title 17, United States Code) governs the making of photocopies or other reproductions of copyrighted material.

Under certain conditions specified in the law, libraries and archives are authorized to furnish a photocopy or other reproduction. One of these specified conditions is that the photocopy or reproduction is not to be "used for any purpose other than private study, scholarship, or research." If a, user makes a request for, or later uses, a photocopy or reproduction for purposes in excess of "fair use" that user may be liable for copyright infringement,

This institution reserves the right to refuse to accept a copying order if, in its judgment, fulfillment of the order would involve violation of copyright law.

Please Note: The author retains the copyright while the New Jersey Institute of Technology reserves the right to distribute this thesis or dissertation

Printing note: If you do not wish to print this page, then select "Pages from: first page # to: last page #" on the print dialog screen

ABSTRACT

THE INCORPORATION OF ELECTROHYDRODYNAMICS AND OTHER MODIFICATIONS INTO A DRY SPINNING MODEL TO DEVELOP A THEORETICAL FRAMEWORK FOR ELECTROSPINNING

by
Yuki Imura

The objective of this research was the development of a mathematical model of the electrospinning process using dry spinning modeling principles as a basis. This model is directed at the identification of parameters which influence final fiber characteristics, e.g., solvent concentration, temperature, spin line tension, and electric field. Preliminary computer simulations were performed; however, the generated data was inconclusive and was determined to be due in part to the complexity of the modeled system and the subsequent computational difficulties encountered. Although a comprehensive computational model of the electrospinning process has not yet been demonstrated, the theoretical development that was undertaken provides a firm foundation for understanding and evaluating the electrospinning process. This development also provides a basis for the future development of a computational model based on this novel approach to electrospinning.

Electrospinning is a method of spinning nanoscale fibers that employs an electric field to propel a stream of polymer solution to create the sub-micron diameter fiber. Although much research has been done on the process itself, its wide-scale adoption has been inhibited by a lack of predictive control on the fiber properties. By developing an accurate computational model, enhanced process control and the production of fibers with desired properties can be attained. A mathematical model of electrospinning was

developed that incorporates dry spinning and electrohydrodynamics principles. The model was based on the premise that the electrospinning of polymer solutions is, in many respects, an extension of dry spinning. Dry spinning is the fiber spinning process where a polymer solution is extruded through a spinneret into a body of circulating air. The air forces the solvent component to vaporize, forming a solid polymer fiber. The model was constructed by incorporating modified components of published 1-dimensional dry spinning and electrospinning models for their treatments of the mass, energy, and electrostatic transport equations. The momentum transport equation was derived independently in order to accurately describe the dynamic conditions unique to the electrospinning regime. This equation also includes terms for electrostatic stresses to account for the electrohydrodynamic interactions between the electrical charges residing on the filament surface and the electrical field. Initial modeling attempts were plagued with issues involving programming and the non-convergence of solutions. The challenge was to properly adapt the aspects of dry spinning to the electrospinning regime. In relation to dry spinning, electrospinning is characterized by high spin line velocities, high strain rates, increased solvent loss rates, and high air drag forces. The extreme changes these quantities undergo within a small length of space, particularly in the initial region just beyond the jet origin, may be a factor in contributing to the numerical instability of the model. Reevaluating the material property formulations and a more robust computational scheme will be considered. The novel incorporation of the principles of electrohydrodynamics (as a mechanism for fluid movement) coupled with very high solvent evaporation rate behavior contributed to a new and representative description of the extreme case of filament diameter reduction inherent in the electrospinning process.

THE INCORPORATION OF ELECTROHYDRODYNAMICS AND OTHER MODIFICATIONS INTO A DRY SPINNING MODEL TO DEVELOP A THEORETICAL FRAMEWORK FOR ELECTROSPINNING

by
Yuki Imura

A Dissertation
Submitted to the Faculty of
New Jersey Institute of Technology
in Partial Fulfillment of the Requirements for the Degree of
Doctor of Philosophy in Materials Science and Engineering

Interdisciplinary Program in Materials Science and Engineering

May 2012

APPROVAL PAGE

THE INCORPORATION OF ELECTROHYDRODYNAMICS AND OTHER MODIFICATIONS INTO A DRY SPINNING MODEL TO DEVELOP A THEORETICAL FRAMEWORK FOR ELECTROSPINNING

Yuki Imura

Dr. Nuggehalli Ravindra, Dissertation Co-Advisor — Date
Professor of Physics, NJIT

Dr. Michael Jaffe, Dissertation Co-Advisor — Date
Research Professor of Biomedical Engineering, NJIT

Dr. Norman Loney, Committee Member — Date
Professor of Chemical Engineering, NJIT

Dr. Treena Arinzeh, Committee Member — Date
Professor of Biomedical Engineering, NJIT

Dr. George L. Collins, Committee Member — Date
Research Professor of Biomedical Engineering, NJIT

Dr. H. Leslie LaNieve, Committee Member — Date
Independent Consultant

BIOGRAPHICAL SKETCH

Author: Yuki Imura

Degree: Doctor of Philosophy

Date: May 2012

Undergraduate and Graduate Education:

- Doctor of Philosophy in Materials Science and Engineering,
  New Jersey Institute of Technology, Newark, NJ, 2012
- Master of Science in Materials Science and Engineering,
  New Jersey Institute of Technology, Newark, NJ, 2003
- Bachelor of Science in Biomedical Engineering,
  Rensselaer Polytechnic Institute, Troy, NY 1994

Major: Materials Science and Engineering

Presentations and Publication

Collins, G., Federici, J., Imura, Y., Catalani, L.H., Charge Generation, Charge Transport, and Residual Charge in the Electrospinning of Polymers: A Review of Issues and Complications, **111**, 044701, J. Appl. Phys. (2012)

Shanmugasundaram, S., Imura, Y., Jaffe, M., Arinzeh, T., Chapter 4: The Contribution of Electrospinning to Tissue Engineering and Related Fields, in: *Tissue Engineering: Roles, Materials, and Applications*, Nova Publishers (2008)

Imura, Y., Wang, X.S., Collins, G., LaNieve, L., Jaffe, M., "An Integrated Model of the Electrospinning Process, The Fiber Society 2007 Spring Conference, Greenville, SC, USA (2007)

This work is dedicated to my Mother and Father, who have given me the love, inspiration and direction to make this all possible. And to my Sisters, who have continually maintained their unwavering support and faith in me. I am truly a person of great fortune and for that I am most grateful.

All I can say now is…ヤッタゼ！*

古人の跡を求めず、古人の求めたる所を求めよ**

松尾芭蕉

* I did it!

**Seek not the paths of the wise;
Seek that which the wise sought.

Matsuo Basho

ACKNOWLEDGMENT

I would like to thank my Co-Advisors, Dr. Nuggehalli Ravindra and Dr. Michael Jaffe, and my committee members, Dr. Norman Loney, Dr. Treena Arinzeh, Dr. George Collins, and Dr. Les LaNieve, for all their guidance and assistance throughout my research. Over the years, I have worked with all the committee members on a variety of levels and I feel I have truly benefited from the diverse fields and backgrounds from which they come. I am especially grateful to Dr. Jaffe and Dr. Collins, who have given me all their time and dedication to my education and personal development from the very beginning, when they accepted me into their laboratory.

A special thank you goes to Dr. Sheldon Wang, who was an integral part of the mathematical modeling aspect of this work and gave me much assistance and encouragement. Thank you also to Dr. Luiz Catalani for inspiring me to always experiment. Thank you to Jean Collins for creating such a pleasant environment for doing good work. To all the MDCL students and colleagues I've known over the years, especially Sherry, Norbert, and Asya – thank you all for your support and friendship. Finally, I'd like to thank my materials science professor, Dr. Roumiana Petrova, who long ago put a seed into my head that I could successfully do doctoral research.

TABLE OF CONTENTS

TABLE OF CONTENTS
(Continued)

LIST OF FIGURES

LIST OF SYMBOLS

A	cross-sectional area, cm^2
C_f	drag coefficient
C_p	heat capacity, erg/(g*K)
E	electrical field, esu/cm^2
E_∞	electrical field, external, esu/cm^2
ε	permittivity, free space, $esu^2/dynes*cm^2$
$\overline{\varepsilon}$	permittivity, air, $esu^2/dynes*cm^2$
g	acceleration of gravity, cm/s^2
γ	surface tension, dynes/cm
h	heat transfer coefficient, $erg/(cm^2*s*K)$
ΔH_{vap}	latent heat of vaporization, erg/g
j	mole fraction, solvent
K	electrical conductivity, filament, s^{-1}
K_a	thermal conductivity, air, ergs/(cm*s*K)
Ky	mass transfer coefficient, $gmol/(cm^{2*}s)$
M	molecular weight, g/gmol
M_{cr}	critical molecular weight, g/gmol
N	molar flux of solvent, $gmol/(cm^{2*}s)$
Nu	Nusselt number
ω	mass fraction
p_2^{sat}	saturation vapor pressure, $dynes/cm^2$

LIST OF SYMBOLS
(continued)

ρ	density, gm/cm^3
ρ_i^0	component density, pure state, g/cm^3
ϕ	volume fraction
η	viscosity, g/cm*s
R	radius, cm
σ	surface charge density, esu/cm^2
T_c	critical temperature, K
T_f	filament temperature, K
T_g	glass transition temperature, K
T_r	reduced temperature, K
v	velocity, cm/s
W	mass flow rate, g/s

Subscripts

1	refers to the polymer component
2	refers to the solvent component
z	with respect to the z position
0	refers to the initial position, *z*=0
a	refers to the air environment

CHAPTER 1

INTRODUCTION

1.1 Objective

Electrospinning is a specialized fiber fabrication method that uses the potential difference of a static electric field as the driving force to propel a fine, charged stream of polymer solution or melt from a capillary orifice to a grounded collection device. The fibers produced can range from 5 microns to 20 nanometers. There are two basic types of electrospinning: polymer solution electrospinning and melt electrospinning. Solution electrospinning is more widely used for its facility and capability of producing nanoscale fibers.

Electrospinning is one of the few known methods of creating nanoscale fibers. Nanoscale fibers are an attractive material for their superior surface area-to-volume ratio, making it ideal for its two major applications as a filtration media[1] and a biomaterial cell substrate.[2-4] The lack of control of desired final fiber characteristics and low throughput have been barriers to the wide-scale adoption and commercialization for use as a scaffolding material for tissue and stem cell engineering applications. This lack of control is not, comparatively, as much as an issue for use as a filtration medium and has therefore seen much more usage and even commercialization in this area.

The advantages of electrospinning over the other methods of nanofiber fabrication are its ease of manufacture, and simple fabrication tools. One of the issues plaguing electrospinning is the lack of control of the final product with respect to fiber diameter, uniformity, and morphology. The inherent instability of the process makes its lack of

repeatability problematic. Throughput is also an issue, as current industrial yield per day is measured in grams, as opposed to industrially melt-spun polyester fibers, which is measured in tons. Underlying these difficulties is the lack of understanding of the fundamentals of the process. The electro-hydrodynamic (EHD) behavior of electrospraying has been extensively studied for decades; however, though similar in many aspects, the electrospinning process has not been characterized and studied as an EHD-driven process in nearly the same way.

1.2 The Electrospinning Process

Electrospinning is an example of an electrohydrodynamic phenomenon. In electrohydrodynamics (EHD), charges induce fluid motion within an electric field. During the process, the transport and distribution of these charges generate stresses that result in the movement of the fluid. Work done in electrohydrodynamics dates back to the early 1900's [5]. However, it was not until the 1930's when Formhals devised a method to create fibers by electrostatic means and thus receive the first patent for the process in 1934 [6]. Since then, the fundamental aspects of the electrospinning process have not changed. As illustrated in Figure 1.1, a high voltage electrode is placed in contact with the polymer solution contained in a pipette or syringe-like vessel with a capillary tip. This electrode provides a source of charge. The ground electrode of the high voltage source is attached to collector plate, which serves as a target for the electrostatically-driven polymer fluid stream. The potential difference between the capillary tip and the ground is typically on the order of 10 to 30kV. At the capillary tip,

the electric field puts a stress on the charged solution and distorts it into a cone-like shape known as the Taylor cone.[7]

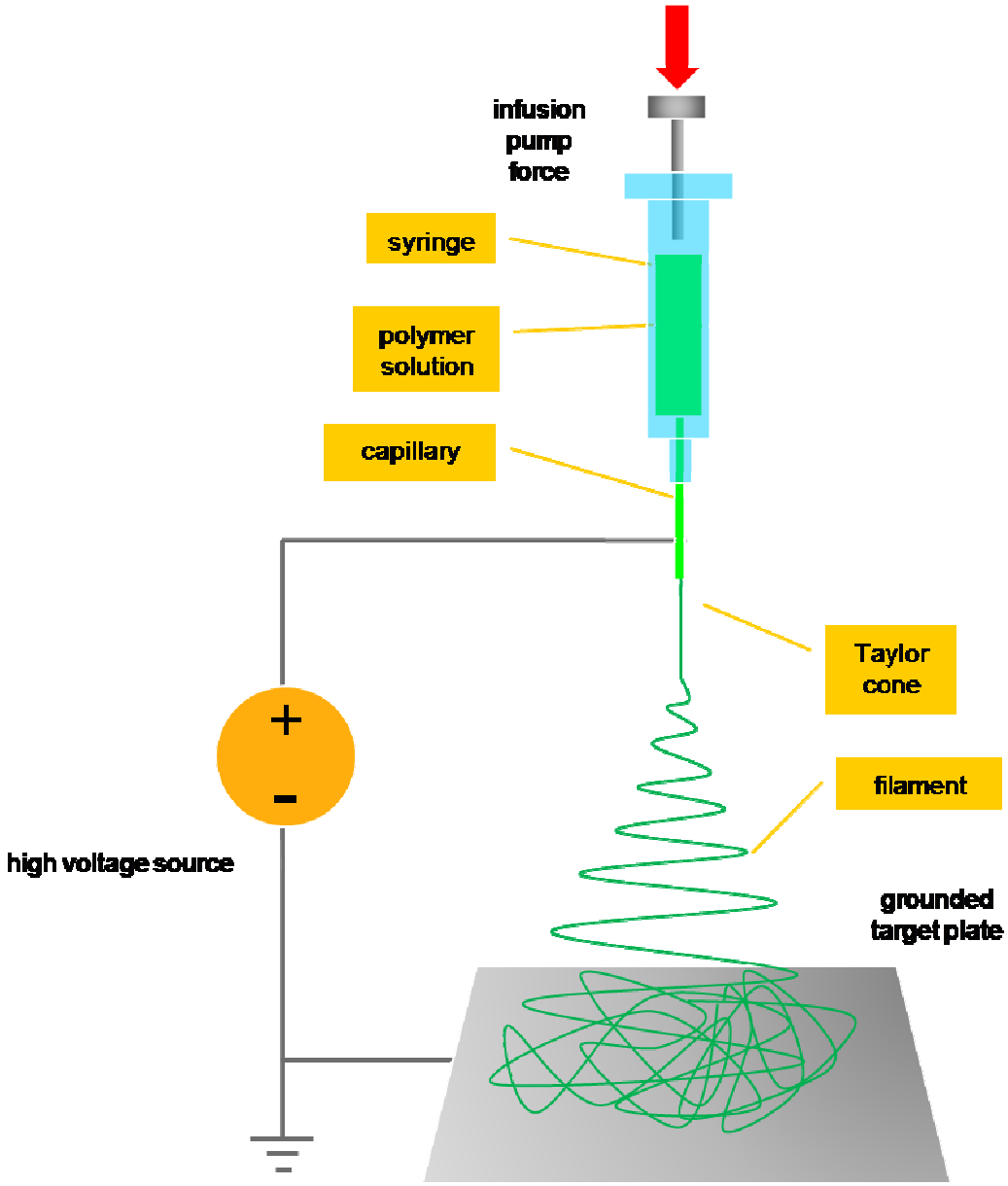

Figure 1.1 A typical electrospinning apparatus configuration.

At a sufficiently high potential difference, the electrostatic stresses overcome the surface tension of the Taylor cone. Then, a stream of polymer fluid is ejected and is propelled towards the grounded target. As the ejected stream forms a filament that traverses the distance from the Taylor cone at the capillary tip to the grounded target, the solvent component is lost by evaporation processes and the remaining polymer solidifies into a coherent filament. The motion of the filament is straight for a relatively short distance and then becomes erratic due to an electric field-induced bending instability. The result of this dynamic process is a non-woven filament mat that collects on the grounded target.

The electrospinning process can be divided into three stages: 1. jet initiation; 2. bending instability; 3. solidification of fiber. [8] Early investigations by Taylor examined the effect of an electric field on a water drop. [9] Taylor did further experiments where he studied the effects of an electric field on liquid jets using various viscous and non-viscous fluids in an electric field and determined the minimum voltage needed to make the fluid jet appear. [10] When a potential difference is applied, positive and negative charges undergo separation within the fluid and charges with the same sign accumulate as the capillary's polarity migrate towards the exposed fluid's bead surface, thereby increasing the surface charge density at the site. The subsequent rise in the local tangential electrostatic stress competes against the surface tension forces holding the bead of liquid together and the hemispherical shape of the bead is transformed into that of an increasing cone-like projection. Once the electrostatic stress dominates, a fluid jet emerges from the apex in order to eject the excess charge within to a lower energy level. Detailed studies focusing on the jet initiation have been performed relating the electrohydrodynamic process to the formation of the cone jet. [7, 11]

Once the jet has initiated, the fluid travels along a straight line for a certain distance. The charged fluid travels towards the collector of the opposite polarity. As the fluid traverses toward the collector, the fluid undergoes an electrically driven bending instability, also referred to as "whipping". The role this bending instability plays in the process is still unclear. Several researchers believe that this bending instability is the most important factor in the formation of small diameter fibers in electrospinning [12]. Shin *et al.* stated that the rapid growth of the non-axisymmetric instability causes bending and stretching of the jet. [12] However, this causal relationship has not yet been conclusively determined by other research.

Three steps in the initiation of the bending cycle were observed: (a) the straight jet forms that was described as a linear array of bends, (b) as the jet elongates, the linear array of bends spirals out with increasing size, and (c) as the spiral grows, the cross-section diameter of the fiber decreases. [13] Although the spiraling fibers appear to be splitting with the naked eye, Baumgarten showed that with the aid of a high speed motion camera, the fibers were actually continuous throughout the process. [14] In addition, extensive use of such equipment by Reneker enabled the discovery of higher order bending instabilities in the jet. [13] As the jet undergoes the process of diameter reduction, its path becomes unstable and a smaller bending instability develops. Three to four successively smaller instabilities have been observed in many cases thus giving the whole instability process a fractal-like configuration,[13] However, Reneker *et al.* have also observed cases where both splitting and bending of the jet due to radial charge repulsion have occurred, thus providing an alternative mechanism for the reduction in fiber diameter. [15]

The solidification of the fiber is a mass transfer process that takes place by the loss of the solvent component out of the polymer solution. There are two possible mechanisms for this loss; conventional evaporation and ion evaporation. Conventional evaporation also called convective mass transfer is a function of the partial pressures of the solvent in the ambient gas phase (usually air) and at the filament surface, as well as the temperatures at those locations. Ion evaporation is the electrostatically-assisted ejection of ionized solvent. [16]

1.3 Dry Spinning

Dry spinning is a spinning process where the polymer solution is extruded through a spinneret. The exiting jets of polymer solution come in contact with a stream of hot gas (typically air). The solvent vaporizes in this gas stream increasing the polymer concentration in the filament and thus solidifying it, as shown in Figure 1.2.

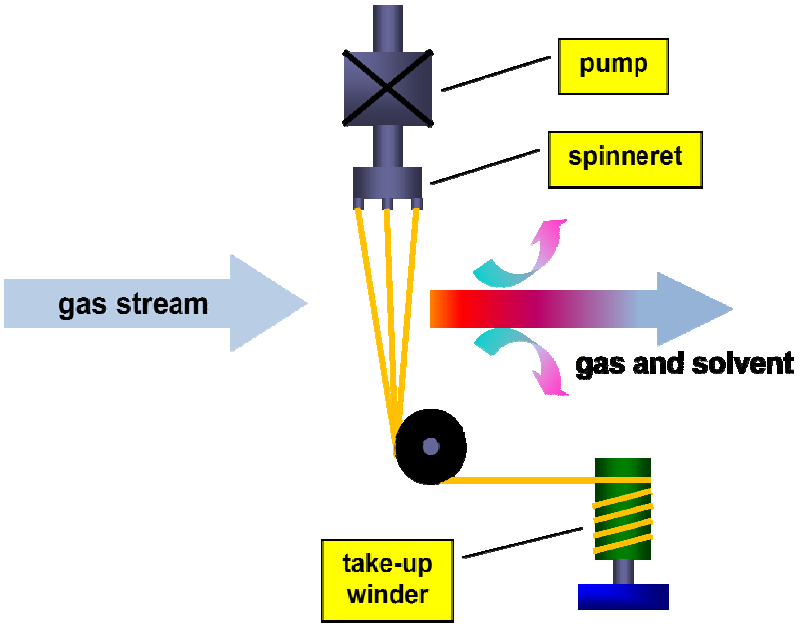

Figure 1.2 The dry spinning apparatus.

1.4 Background and History

Work on this research began with an extensive review of the literature on dry spinning and electrospinning modeling. The initial step was the literature review of the dry spinning models. In dry spinning, the fibers exhibit certain morphological qualities that arise from radial variations in temperature and solvent concentrations. Brazinsky *et al.* [17] developed a two-dimensional model of a cellulose acetate/acetone dry spinning system that takes those variations into account and the results from the model were compared with the experimental data. Based on the review of this paper, questions arose whether those axial and radial variations existed in electrospinning and to be safe, a two-dimensional electrospinning should also be made. However, it was realized that robust and practical one-dimensional electrospinning model capable of generating detailed profiles for radius, solvent concentration, and temperature did not really exist and that it may be more prudent to create a simpler one-dimensional model in the beginning and build-up the complexity later on. Therefore, a one-dimensional dry spinning model by Ohzawa *et al.* [18] was reviewed. This model's unique characteristic was the assumption that the tension was constant throughout the spin line. Another one-dimensional dry spinning model by Gou[19] was reviewed which focused on understanding the solidification mechanism and the prediction of the solidification point. In addition, this model also included comparisons of the predictions of the jet behavior for both the Newtonian and viscoelastic constitutive cases.

The published models on the electrospinning process can be categorized by the portion of the electrospinning process that was studied. The process can be divided into three groups. The first group is the Taylor cone and the jet initiation from the fluid bead.

The second group is the straight-line portion of the jet. The third group is the bending instability portion. Because the objective for the model was the determination of certain parameter profiles, the focus was on the portion of the jet beyond the apex of the Taylor cone. However, in order to comprehensively understand the nature of the process, a review of the literature on the jet initiation[10, 11] and the fluid mechanics of the Taylor cone [20] was done.

Review of the papers on the straight-line portion of the jet began with the model by Spivak and Dzenis [21] that was a simplified view of the process with its assumption that the electric field is constant, despite the charge density gradients on the jet. Work by Hohman *et al.* [22] introduced the slender-body theory that accounts for the effects of jet stretching, charge transport, and the electric field. Feng [23] describes a similar model to the one developed by Hohman *et al.* with some key modifications that avoided the instability issues with the Hohman *et al.* model. More significantly, Feng's derivations for the electrostatic forces on the jet, which coupled the charge density effects on the tangential traction forces on the jet, were consistent with the conceptualization of the diameter reduction mechanism. Therefore, several expressions for the electrostatic force were adopted for use in our model.

The bending instability portion has been studied in detail by several groups. Reneker *et al.* [15] modeled the jet by a linear Maxwell equation and have suggested that the jet undergoes bending instability arising from the repulsive forces from the charged ions within the jet. These forces have a destabilizing effect on the jet. Shin *et al.* [12] based their model of the instability on the competition of several classes of instabilities which are influenced by the interaction of ions and the electric field. These instabilities were

found to vary with respect to the location on the path depending on the jet material parameters and the operating conditions. Along similar lines, Hohman *et al*. [22] developed an electrohydrodynamic theory for the instability behavior. The theory predicts that, at increased field strengths, the electrical non-axisymmetric instability is dominant over the Rayleigh instability and is dependent on the surface charge density and the jet radius. Fridrikh *et al.*[24] re-examined the model equations of Shin *et al.* to create a model to determine the final diameter of the fiber by including nonlinear instability effects of the bending instability as a function of surface tension, flow rate, and the electrical current within the jet. Although this particular work is very similar in its goals with those of the research in this thesis with respect to the prediction of jet radius, the Fridrikh *et al.* model did not include solvent evaporation effects and the mechanism for diameter reduction was suggested to be as a result of the bending instability.

So far, the electrospinning models that have been published did not simulate solution electrospinning for high evaporation rate solvents. In certain cases, oversimplifications of the parameters were done resulting in data that may have limited use in the further understanding of the process. Still other models tended to focus on the behavior and the simulation of the bending instability aspect, rather than the roles mass transfer and the electrostatics play in influencing the diameter reduction of the jet. The researched model is unique in that it encompasses the entire physical range of the process, from the capillary exit to the nanoscale fiber at the collection plate.

CHAPTER 2

THE ROLE OF ELECTROHYDRODYNAMICS IN ELECTROSPINNING

2.1 Electrospinning: An Electrohydrodynamic Phenomenon

Electrospinning is an electrohydrodynamic phenomenon where charges induce fluid motion within an electric field. During the process, the transport and distribution of these charges generate stresses that result in the movement of the fluid. Studies on the electrostatic forces involved in electrospinning are relatively fewer in amount compared to the number of applications-oriented electrospinning papers published today. However, the field of electrohydrodynamics (EHD) and specifically the studies on the electrospray process, which is process-wise very similar to electrospinning, provide a rich source of information that clarifies the complex characteristics and behavior of the electrostatic forces involved in electrospinning.

2.2 Development of Electrohydrodynamics

EHD is the study of electric field-induced fluid motion. It is the dominant phenomenon that allows the polymer solution to be stretched into a fine, continuous filament in the electrospinning process. The focused study on EHD began in the 1960's with Taylor's investigation into the circulation produced within a dielectric fluid body in the presence of an electric field.[25] The resulting observations supported the notion of the unique property of dielectrics where charges would reside at the interfaces of two substances with different permittivities. The field of EHD also includes the areas of electrostatics, fluid dynamics, and electrokinetics. Electrokinetics is the study of charged particles in

aqueous electrolytes. This phenomenon is dominated by a diffuse charge-induced concentration gradient at an interface, resulting in counteracting electromigration effects. With leaky dielectrics, these conditions do not exist. Therefore, although these two areas had fundamental processes in common, they were developed separately. The two treatments began to develop into a single approach with the paper by Melcher and Taylor (1969). [26] The purpose of that study was to address some of the weaknesses of EHD research at the time, including lack of reproducibility of experiments and the inadequacies of theoretically-based models. Adopting the techniques used in the study of fluid mechanics by investigating the relationship between experimental data and analytical models, an investigation into the behavior of regions of fluids with uniform ohmic conductivity and permittivity and the influence of interfacial electrical shear-force densities on their surface interactions was performed. [27]

2.3 The Leaky Dielectric Model

This leaky dielectric EHD model is an appropriate model to use because the model of the fluid's electrical properties as a poorly conducting liquid is comparable to the behavior of most polymer solutions, the most commonly-used type of fluid in electrospinning. The leaky dielectric model is composed of the Navier-Stokes equations to describe fluid movement and a formulation of a current balance equation. Electromechanical coupling, the core of EHD behavior, occurs only at the fluid-to-fluid interfaces. The charges transported via conduction reside at these interfaces and their subsequent presence at these locations produce electrical stresses that differ from those in perfect dielectrics or perfect conductors. For these media, the stresses act normal to the interface and are

subsequently balanced by changing the shape of the interface and interfacial tension. However, these models cannot explain the observed nature of very fine steady jets relative to their meniscus [28] or just the basic phenomena of fluid movement in an electric field. The reason is that, for example, a perfect dielectric still contains a finite amount of free charge density. Although this charge density may be small enough to ignore bulk conduction effects, the charge will reside on the interfaces between fluids. If a nonzero electric field is tangent to the interface, then a nonzero tangential stress will be induced on the interface. The only possible force that can balance this tangential stress is viscous and therefore, under these conditions, such a fluid will be in motion. [22]

In 1966, Taylor [25] initiated the development of a new model for poorly-conducting fluids, or leaky dielectrics, where the free charge accumulates at the interfaces, due to adjacent fluids having different conductivities, to modify the electric field and preserve the conservation of current. The field-induced tangential stress components are then balanced by viscous fluid motion which ultimately leads to steady cone-jet formation. [26, 28] This leaky dielectric model assumes that the medium behaves as an ohmic conductor, where the electrical conductivity is constant. This charge transport model combined with the Navier-Stokes equations of motion became the leaky dielectric model. [28]

The effects of the tangential forces on the fluid body has been observed and studied. Circulatory fluid motion induced by an electric field was observed in the works of Taylor. [25, 27] Tangential stresses arising from charge conduction to the interface initiated the circulation patterns inside and outside the drop. These accumulations of charge stem from differences between the conductivity of the interior and exterior fluids.

A circulation pattern also exists within the Taylor cone with fluid moving towards the apex along the cone surface (i.e., the interface between the two media) and away from it along the axis. The fluid is supplied to the jet from the surface of the cone, while a recirculating eddy current moves fluid down the axis of the cone back towards the supply.[26]

2.4 Formulation of the Leaky Dielectric Model

The validity of using electrostatic equations for the leaky dielectric model approximation is determined by whether the electrical relaxation time fulfills certain inequality relationships. The electrical relaxation time, τ_e, is the ratio of the permittivity ($\varepsilon\varepsilon_o$) and conductivity (σ). Transport process time, or the hydrodynamic time, τ_h, represents the time required for fluid particles to move across a zone of space. If τ_e is much smaller than τ_h, the liquid bulk is quasi-neutral and the free charges are confined to a very thin layer under the liquid-gas interface. In cone-jet mode electrosprays, charges have to be relaxed at the cone-jet surface since any motion of charges inside the liquid bulk would result in being incompatible with the stability of the cone-jet mode. [29] Therefore, the inequality of $\tau_e \ll \tau_h$ must be satisfied in electrospray atomization, and by extension, the electrospinning process.

It is important to understand how this electromechanical coupling takes place by describing how certain key components of the leaky dielectric model were formulated. It is the Maxwell stress tensor that couples the electrostatic phenomena and hydrodynamic behavior. This can be understood by supposing that electrical forces exerted on free charge and charged dipoles are transferred directly to the fluid. With dielectrics, steady

current cannot flow in them. Therefore, unlike conductors, the static electric field is not zero and can be derived.[30] The following derivation is based on Ref. [31] and Ref. [26]. Starting with modified Maxwell's equations representing electrical phenomena: $\nabla \bullet \varepsilon \varepsilon_o \mathbf{E} = \rho^e$ and $\nabla \times \mathbf{E} = \mathbf{0}$ with electric field, E, the total charge density, $\rho^{(e)}$, permittivity, ε, and the permittivity of the vacuum, ε_o.

Electric fields polarize matter in two ways: by orienting molecules with permanent dipoles and by deforming electron clouds within individual atoms and molecules. The polarization vector, $\mathbf{P}$, is defined with respect to individual dipoles by $\mathbf{P} = NQ\mathbf{d}$ where, N is the number of dipoles per unit volume, Q is the charge magnitude separated to produce the dipole, and $\mathbf{d}$ is the dipole orientation. Additionally, this polarization vector not only describes the volumetric charge density but also the surface charge density qualities[30].

$$\mathbf{P} = \mathbf{N}\alpha\varepsilon\varepsilon_o\mathbf{E} \tag{2.1}$$

The polarization vector is then used to define the volumetric polarization charge density $\rho^{(p)}$ as,

$$\nabla \bullet \mathbf{P} = -\rho^{(p)} \tag{2.2}$$

It is also necessary to define the stress that an external field exerts on a surface. This is done by first deriving the force due to electric field acting on an isolated dipole. A pair of charges, Q and $-Q$, are at some position $\mathbf{d}$. Then the electrical force on the pair is $-Q\mathbf{E}(\mathbf{x}) + Q\mathbf{E}(\mathbf{x} + \mathbf{d})$. Expanding the second term and taking limits yields the expression for the force on an individual dipole, $(Q\mathbf{d}) \bullet \nabla \mathbf{E}$. For N dipoles per unit volume, the dipole

force is $\mathbf{P}\bullet\nabla\mathbf{E}$. The Coulomb force due to free charge is $\rho^{(f)}\mathbf{E}$. Therefore, the total electrical force per unit volume is $\rho^{(f)}\mathbf{E}+\mathbf{P}\bullet\nabla\mathbf{E}$. These are body forces that have to be balanced by the pressure gradient, $-\nabla p^*$, yielding $-\nabla\rho^*+\rho^{(f)}\mathbf{E}+\mathbf{P}\bullet\nabla\mathbf{E}=0$. Using the expressions relating charge and dipole density to field strength, (2.1) and (2.2), the force terms can be transformed into an expression of the divergence of a tensor[31]:

$$-\nabla p^*+\nabla\bullet\left(\varepsilon\varepsilon_o\mathbf{E}\mathbf{E}-\tfrac{1}{2}\varepsilon\varepsilon_o\mathbf{E}\bullet\mathbf{E}\delta\right)=0 \tag{2.3}$$

The pressure p^* is due to the isotropic influence of the electrical field, i.e. electrical modifications to the short-range intermolecular forces. Pressure in the absence of an electric field owing to kinetic energy and short-range intermolecular forces is defined as p so as to give the relation:

$$p^*=p+\tfrac{1}{2}\varepsilon_o\left[\varepsilon-1-\rho\left(\frac{\partial\varepsilon}{\partial\rho}\right)_T\right]\mathbf{E}\bullet\mathbf{E} \tag{2.4}$$

where, ρ is the density of the material and the derivative $\left(\frac{\partial\varepsilon}{\partial\rho}\right)$ is taken at constant temperature, *T*. Determining the gradient and the divergence of the total stress in eauation (2.3) yields[31]

$$-\nabla p+\nabla\bullet\left\{\varepsilon\varepsilon_o\mathbf{E}\mathbf{E}-\tfrac{1}{2}\varepsilon_o\varepsilon\left[1-\frac{\rho}{\varepsilon}\left(\frac{\partial\varepsilon}{\partial\rho}\right)_T\right]\mathbf{E}\bullet\mathbf{E}\delta\right\}=0 \tag{2.5}$$

.

The tensor within the braces, $\{\ \}$, is the Maxwell stress tensor, σ^M. The gradient of the pressure along with the divergence of the stress tensor are components of the equation of motion for an incompressible Newtonian fluid of uniform viscosity:

$$\rho\frac{D\mathbf{u}}{Dt} = -\nabla p + \nabla\bullet\sigma^M + \mu\nabla^2\mathbf{u} \tag{2.6}$$

where, $\mathbf{u}$ is the fluid velocity and μ is the viscosity. Solving for the gradient and the divergence in equation (2.5) shows how the electrical stresses emerge as body forces due to heterogeneous permittivities and distribution of free charges and with the gradient of the pressure yields [26] the following:

$$\rho\frac{D\mathbf{u}}{Dt} = -\nabla\left[p - \tfrac{1}{2}\varepsilon_o\rho\left(\frac{\partial\varepsilon}{\partial\rho}\right)_T \mathbf{E}\bullet\mathbf{E}\right] - \tfrac{1}{2}\varepsilon_o\mathbf{E}\bullet\mathbf{E}\nabla\varepsilon + \rho^{(f)}\mathbf{E} + \mu\nabla^2\mathbf{u} \tag{2.7}$$

Equation (2.7) describes how the electrostatic forces cause the fluid jet to move. For a detailed description of the derivation, please refer to Ref. [31] and Ref. [26]. A summary of the leaky dielectric equations can be found in Ref. [26].

2.5 Validation and Assessment of the Model

Taylor's initial efforts in the leaky dielectric theory [25] in the study of drop deformations led to a function to determine if deformations were either prolate or oblate. Subsequently, this function led to a derivation of a scaling law for drop deformation, thus allowing for

the theory to be evaluated quantitatively. Taylor did not publish a comparison between theory and experiment and the first quantitative tests were done by Torza *et al*., in which the theory was applied to alternating fields as well as steady fields. [32] The results showed that although the theory was qualitatively sound, the quantitative agreement was very poor.

Attempts were made by several researchers to improve the agreement between theory and experiment but they were met with varying success. Ref.[33] extended the model by replacing the ohmic property with electrokinetic effects. The assertion is that the ions are constantly mobile whose concentrations are governed by transport equations. However, the results were identical to the original theory. Other studies such as Ref.[34] and Ref.[35] have taken steps to increase the accuracy of the measurements of certain physical properties, e.g., permittivity, and used novel techniques like finite element method to analyze the drop deformation, respectively. In the end, the original ohmic model appears to remain valid and is satisfactory for drop deformation cases.

Studies on electrified fluid cylinders and free jets, which are the modes of electrospinning, were done to investigate stability behavior. [10] The leaky dielectric model was applied for a case of a viscous cylinder immersed in another viscous fluid under simplified conditions where charge transport by relaxation, convection and dilation of the surface were neglected.[26] The results showed reasonable agreement with the behavior described in Ref.[10]. However, certain characteristics could not be captured because of the simplified conditions used. These omissions were determined to be critical in the description of the jet stability and were recommended to be included in further analysis [36].

Overall, the leaky dielectric theory's qualitative analysis is consistent with the experimental data provided in Taylor's 1969 study of electrically driven jets [26].

2.6 Electrospinning: An Extension of Electrospraying

The physical phenomena of electrospinning share many similarities with those of electrospraying. This has allowed researchers to take advantage of the vast body of literature in the area of electrospray characterization to supplement the comparatively smaller amounts of relevant information available for electrospinning. When a potential is applied to a spheroidal meniscus of fluid, charges migrate to the surface and create tangential stresses that deform the meniscus into a cone-like projection, or Taylor cone, at the limit of stability [26]. Further increases in tangential stresses pull the charged surface towards the tip of the cone providing sufficient axial momentum transfer to further deform the Taylor cone to eject a fluid jet. [29] Depending on certain conditions, the meniscus may eject charged droplets, emit a jet that disperses into drops, or emit a continuous jet that would eventually become a fiber [37]. The level of balance between the electrostatic stresses and surface tension is what determines the outcome.

In electrospraying, a Taylor cone is formed at the tip of a capillary from which jets a stream of fluid. This electrically driven jet is inherently unstable and it undergoes instability modes due to either capillary instabilities resulting in break up into charged droplets or in the case of electrospinning, tornadic instabilities, i.e., whipping mode, due to the action of the electric field [38]. In electrospinning, formation of continuous fibers can be achieved by suppressing the capillary instability through, for an example, the use of polymer solutions of certain levels of viscosity to rheologically dampen, delay, or even

eliminate the axisymmetric perturbations so that longer jets may be obtained. However, non-axisymmetric perturbations may still persist and even grow because of the charges that are still carried by the jet. The tangential stresses generated serve to further deform a portion of the jet so that it intersects with the electrical field lines inducing charge[26]. Surface charge density gradients that have developed due to this action push that portion farther away from the original axis creating the observed tornadic instabilities known as whipping, or bending instabilities. [38]

CHAPTER 3

BUILDING THE PRELIMINARY MODEL

The differences between the processes of dry spinning and electrospinning are both obvious and subtle. In dry spinning, the fluid undergoes die swell upon exiting the spinneret. This is a consequence of the relaxation of the fluid molecules. This phenomenon does not occur in electrospinning because of the comparatively low flow rates used. In addition, the mechanically metered flow rates are not necessary for the primary propagation of the electrospinning process. It only serves a secondary role to supply the capillary tip with fresh polymer solution. The spinneret size in dry spinning is an important factor in determining the final diameter of the filament. However, in electrospinning , the only role the spinneret, or in this case, the capillary, plays is as a charge generation device. The most significant difference is the method of filament traction. In dry spinning, this is done by the use of a "take-up" winder assembly, which provides a mechanical traction to the spin line. In electrospinning, the sole source of traction is by electrostatic means, generated by the electrohydrodynamics interaction of the surface charges residing on the filament surface and the surrounding external electric field. However, the two processes are similar in major aspect. The solvent loss mechanisms are primarily by evaporation. Although dry spinning also includes diffusion as an important mechanism of solvent loss, the effect is neglected in electrospinning due to its relatively small fiber diameters.

3.1 Modeling the Dry Spinning and Electrospinning Processes

Work on the solution for the electrospinning model began by first repeating the 1D dry spinning model by Gou [19] to learn and verify the modeling approach. A model was formulated based on the published balance equations and the material property relationships. Full profiles for solvent fraction, radius, velocity, and temperature were generated for a Newtonian fluid model shown in Figure 3.1. Although the individual numerical values differed, the overall plot behavior and profiles closely approximated those published and so work progressed to the next stage.

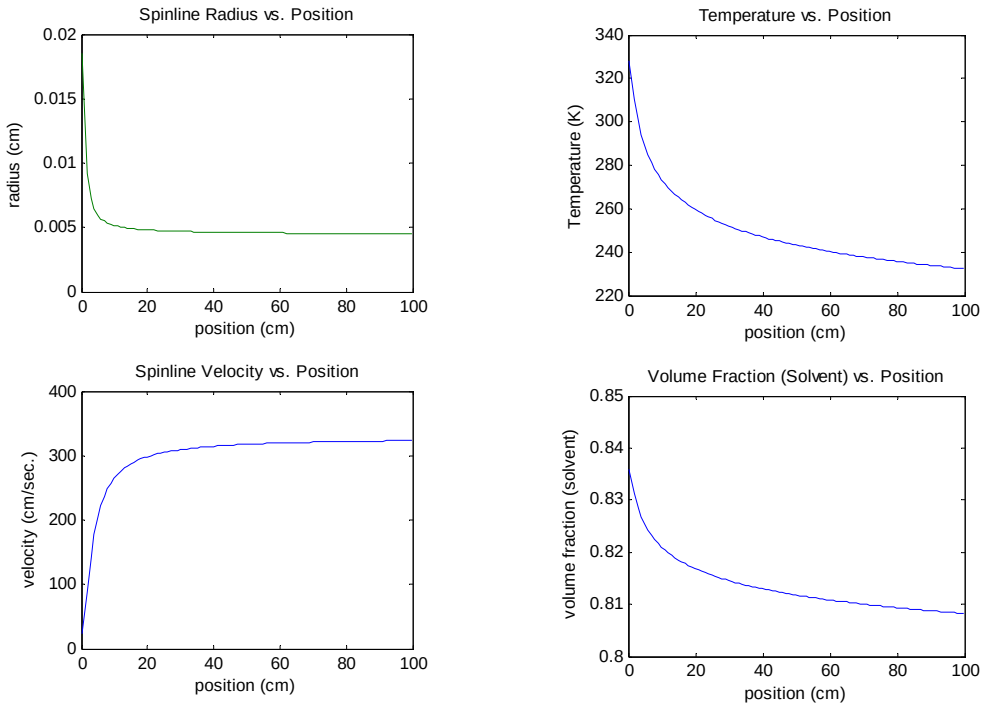

Figure 3.1 Initial results of the dry spinning model.

Work on the actual electrospinning model began with the selection of Feng's electrostatic formulations for the force and axial electric field.[23] These equations were derived by

coupling the charge density effects on the tangential traction forces on the jet. The significant role surface charge density plays in the electrostatic force terms could be clearly seen and understood, in comparison to the other published models, and therefore led to its inclusion in the proposed model. Feng's equations were to a certain extent, similar to Hohman's model.[22] The difference lay in Feng's use of an approximation to one of Hohman's more complex equation in order to avoid the instabilities that characterized the Hohman *et al*. model at the initial stages of the simulation. The source of the problem was the boundary condition for the charge density, whose solution existed for a very narrow range. The use of Feng's equation allowed for a stable solution to be achieved with the only requirement that the boundary condition for the electrical field and the charge density be defined initially.

For the solution to the electrospinning model, five balance equations were made for mass, momentum, energy, axial electrical field, and the charge. The mass, momentum, and energy balance equations were from the Gou dry spinning model, with the last three terms of the momentum balance equation taken from the Feng model, as were the axial electric field and the charge balance equations. The mass balance equation describes the change in the solvent concentration with respect to the spin line position, *z*, in terms of the material properties that influence solvent evaporation, e.g. the mass transfer coefficient, *ky*, and the saturation vapor pressure, p_2^{sat}. The momentum balance equation describes the change of the spin line velocity with respect to *z*, in terms of the rheological, gravitational, surface tension, air drag, and electrostatic forces. The energy balance equation describes the change of the spin line temperature with respect to *z*, in terms of the interfacial temperature gradients, heat loss through vaporization, and

rheological heating. The electric field balance equation describes the change in the internal, axial electrical field with respect to z, in terms of the external electric field and the charge densities. The charge balance equation gives a description of the total current in terms of the current flows in the interior and exterior regions of the jet. These equations are ordinary differential equations with respect to one independent variable, the position on the spin line, *z*. Therefore, the model is considered a one-dimensional model, where the parameters depend only on the *z* position and not on the radial position. At this time, it is unknown if radial dependencies of the material properties exist thereby not justifying the creation of a more complex, two-dimensional model. Additionally, in the early stages, it was decided to keep the model as simple as possible and gradually build up the complexity as progress was made.

The program was a modified version of the one written for the dry spinning modeling work done earlier. In the interest of simplicity, as in the dry spinning model, a Newtonian fluid model was used along with a Runge-Kutta 2^{nd} order numerical integration scheme. The modeled fluid was 8% by mass of cellulose acetate to acetone, a very common polymer solution system used in dry spinning. During this initial period, plausible profiles for radius, velocity, surface charge density, temperature, and solvent volume fraction were made. However, subsequent investigations into the model revealed numerous errors in the fundamental components of the model. These errors include those made to the formulation for the mass flow rate, the incomplete conversion of material property units from MKS to CGS dimensions, and also errors discovered in the referenced literature. After all the known errors had been rectified, the program still did

not run, which indicates a fundamental error in the program, the formulation of the parameters, or both. The equations used for the preliminary electrospinning model were:

$$\frac{d\phi_2}{dz} = \frac{-2\hat{v}_2 k_y M_2 (1-\phi_2)}{r V_z}\left[\frac{a_2 P_2^{sat}}{P} - y_{2g\infty}\right]$$

$$\frac{dT}{dz} = \frac{-2}{r\rho C_p V_z}\left[h(T-T_a) + \Delta H_v k_y M_2 (a_2 \frac{P_2^{sat}}{P} - y_{2g\infty})\right]$$

$$\frac{dv_z}{dz} = \frac{1}{\rho v_z A}\left[\rho A g + \frac{d\left(3\eta_0 A v_z'\right)}{dz} + \pi\gamma\frac{dR}{dz} - \pi R C_f \rho_a \left(v_z - v_a\right)^2 + A\frac{\sigma\sigma'}{\varepsilon} + A(\varepsilon-\bar{\varepsilon})EE' + \pi 2R\sigma E\right]$$

$$\frac{dE}{dz} = \frac{R}{4}\left(\frac{dR}{dz}\right)^{-1}\left[\frac{2}{R^2\beta}\left[\frac{E(z)-E_{\infty(z)}}{\ln\chi} + \frac{1}{\bar{\varepsilon}}\frac{d(\sigma R)}{dz}\right] - \frac{d^2E}{dz^2} - \frac{2E}{r^2}\left(\frac{dR}{dz}\right)^2 - \frac{2E}{r}\frac{d^2R}{dz^2}\right]$$

CHAPTER 4

THE NEW MODEL

The governing transport equations are the mass, energy, and the momentum transport equations. Additionally, the electrospinning model requires the current conservation equation and the expression for the axial electrical field within the filament bulk. The modeled portion of the filament, called the differential volume element (DVE), is shown in Figure 4.1. First, the material balance equations are defined.

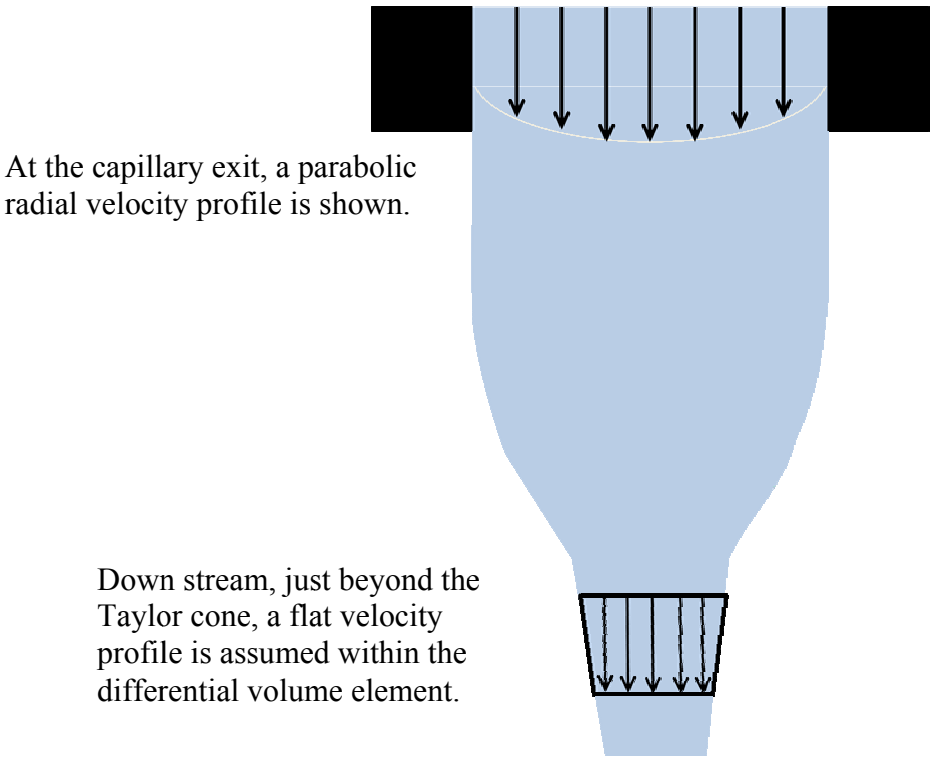

Figure 4.1 A macroscopic view of the modeled portion of the electrospinning process.

4.1 The Material Balance Equation:

The total mass flow through the system is given by,

$$W = W_1 + W_2$$

The mass flow rate of the polymer component (W_1) throughout the system is constant, whereas the mass flow rate of the solvent component (W_2) changes with z due to mass transfer by evaporation.

$$W_1 = \rho_f \omega_1 \pi R^2 v_z \tag{4.1}$$

from which the equation for radius, R, is derived

$$R = \left[\frac{W_1}{\rho_f \omega_1 \pi v_z} \right]^{\frac{1}{2}}$$

4.2 The Mass Balance Equation

The derivation of the mass transport equation closely follows the one given in Ohzawa. [18] The physical description is shown in Figure 4.2. The equation follows the form:

$$\begin{pmatrix} \text{mass rate} \\ \text{of accumulation} \end{pmatrix}_2 = \begin{pmatrix} \text{net mass} \\ \text{flow rate} \end{pmatrix}_2 + \begin{pmatrix} \text{solvent mass} \\ \text{loss rate} \end{pmatrix}_2$$

The derivation is begun by first defining the component mass fraction relationship:

$$\omega_1 + \omega_2 = 1 \tag{4.2}$$

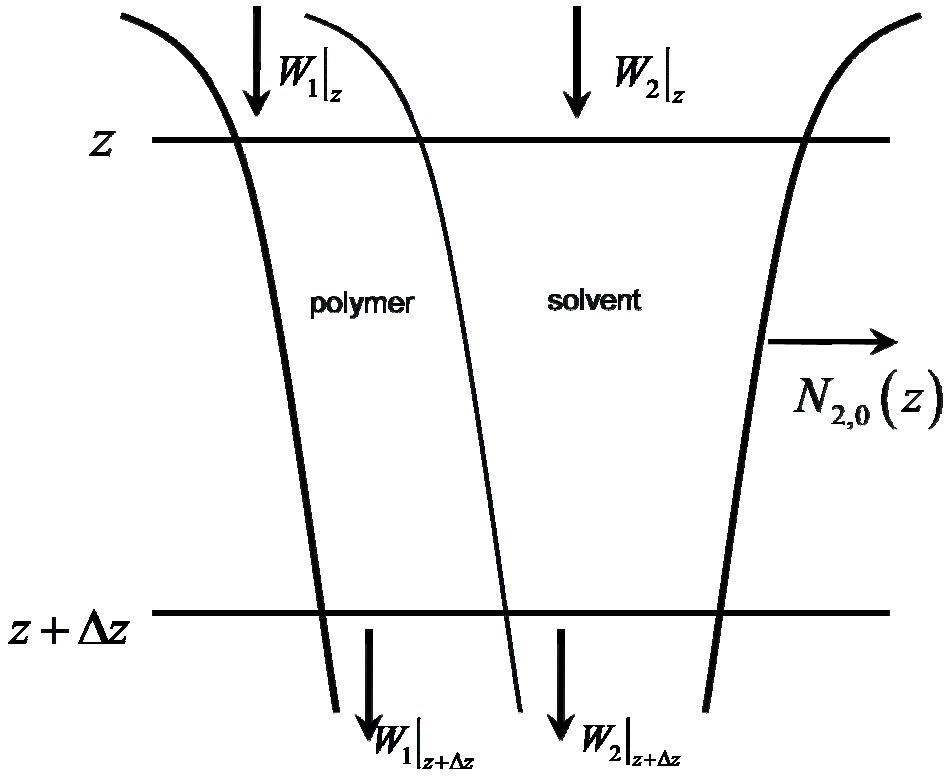

Figure 4.2 Differential volume element for the macroscopic mass balance.

Assumptions were made to restrict the scope of the equations to the desired modeled conditions.

Assumption 1: The filament cross section is circular and axi-symmetric.

Assumption 2: The filament concentration distribution of binary components is uniform throughout. Therefore the filament density is constant in the radial direction.

The mass flow rate of the polymer entering the z-plane at time t is:

$$W_1(z,t) = \int_0^R 2\pi r \rho \omega_1 v_{1,z} dr \tag{4.3}$$

The mass flow rate of the solvent entering the z-plane at time t is:

$$W_2(z,t) = \int_0^R 2\pi r \rho \omega_2 v_{2,z} dr \tag{4.4}$$

Adding equations (4.3) and (4.4) gives the total mass flow rate:

$$W(z,t) = W_1(z,t) + W_2(z,t) \tag{4.5}$$

In reference to Figure 4.2, a macroscopic mass balance of the polymer component over a differential volume element (DVE) bound by the z and $z + \Delta z$ is as follows:

The total mass of the polymer component in the DVE is:

$$\left(\int_0^R 2\pi r \rho \omega_1 dr \right) \bullet \Delta z \tag{4.6}$$

The rate of mass accumulation of the polymer component in this DVE is:

$$\left[\frac{\partial}{\partial t} \left(\int_0^R 2\pi r \rho \omega_1 dr \right) \right] \bullet \Delta z \tag{4.7}$$

The total input of the polymer component across the z plane is:

$$W_1(z,t) \tag{4.8}$$

The total output of the polymer component across the $z + \Delta z$ plane is:

$$W_1(z+\Delta z,t) \tag{4.9}$$

Then the mass balance becomes,

$$\left[\frac{\partial}{\partial t}\left(\int_0^R 2\pi r\rho\omega_1 dr\right)\right]\bullet\Delta z = W_1(z,t) - W_1(z+\Delta z,t) \tag{4.10}$$

By dividing both sides by Δz and taking the limit as Δz approaches zero, the continuity equation for the polymer component is given by,

$$\frac{\partial}{\partial t}\left(\int_0^R 2\pi r\rho\omega_1 dr\right) + \frac{\partial W_1}{\partial z} = 0 \tag{4.11}$$

In electrospinning, the mechanism of mass transfer by diffusion is considered to be negligible due to the characteristically small diameters found in the process.

Assumption 3: Solvent mass transfer is by the process of evaporation only. Diffusion is considered to be negligible.

The solvent transfer in the gas phase from the filament interface follows the principles of the Whitman 2-film theory.[18]

The rate of solvent transfer at the interface is given by the molar flux, $N_{2,0}$:

$$N_{2,0} = ky\left(j_{2,0} - j_{2,\infty}\right)\Big/\left(1 - j_{2,0}\right) \tag{4.12}$$

where, ky is the mass transfer coefficient, $j_{2,0}$ is the mole fraction of the solvent vapor, and $j_{2,\infty}$ is the mole fraction of the ambient air.

The rate of total mass accumulation of the solvent component in the DVE is:

$$\left[\frac{\partial}{\partial t}\left(\int_0^R 2\pi r\rho\omega_2 dr\right)\right]\bullet\Delta z \tag{4.13}$$

Total input of the solvent component across the z plane is:

$$W_2\left(z,t\right)$$

Total input of the solvent component across the z+ Δz plane is:

$$W_2\left(z+\Delta z,t\right)$$

Evaporation rate of solvent across the filament/air interface is:

$$M_2 N_{2.0} \bullet 2\pi R\Delta z$$

By dividing both sides by Δz and taking the limit as Δz approaches zero, the continuity equation for the solvent component is given by,

$$\frac{\partial}{\partial t}\left(\int_0^R 2\pi r\rho\omega_2 dr\right) + \frac{\partial W_2}{\partial z} + 2\pi R M_2 N_{2,0} = 0 \tag{4.14}$$

Adding equations (4.11) and (4.14) gives the continuity equation for the polymer solution:

$$\frac{\partial}{\partial t}\left(\int_0^R 2\pi r\rho dr\right) + \frac{\partial W}{\partial z} + 2\pi R M_2 N_{2,0} = 0 \tag{4.15}$$

Then, substitute equations (4.3) into (4.11) and divide both sides by W_1

$$\frac{1}{\omega_1}\bullet\frac{d\omega_1}{dz} + \frac{1}{A}\bullet\frac{dA}{dz} + \frac{1}{v_z}\bullet\frac{dv_z}{dz} = 0 \tag{4.16}$$

Then, substitute equation (4.4) into equation (4.14) and divide both sides by W_2

$$\frac{1}{\omega_2}\bullet\frac{d\omega_2}{dz} + \frac{1}{A}\bullet\frac{dA}{dz} + \frac{1}{v_z}\bullet\frac{dv_z}{dz} + \frac{2\pi R M_2 N_{2,0}}{W_2} = 0 \tag{4.17}$$

By subtracting equation (4.17) from equation (4.16), an ordinary differential equation is determined for the mass fraction of the solvent:

$$\frac{d\omega_2}{dz} + \frac{2\sqrt{\pi}M_2}{W_1} \bullet \sqrt{A} N_{2,0} \left(1-\omega_2\right)^2 = 0 \tag{4.18}$$

4.3 Energy Balance Equation

The energy transport equation is also adopted from Ohzawa[18] and follows the law of conservation of energy over the DVE as shown in Figure 4.3.

The macroscopic energy balance equation follows the form:

$$\begin{pmatrix}\text{rate of accumulation}\\ \text{of energy}\end{pmatrix} = \begin{pmatrix}\text{net energy}\\ \text{flow rate}\end{pmatrix} - \begin{pmatrix}\text{heat loss by}\\ \text{evaporation}\end{pmatrix} + \begin{pmatrix}\text{heat transfer}\\ \text{from environment}\end{pmatrix}$$

Assumption 3: Energy transport by radiation and by conduction in the z-direction is negligible.

Assumption 4: Kinetic energy contributions and work done by forces due to pressure, gravity, viscous, drag, and electrohydrodynamics are negligible.

The spinning medium is a polymer solution; therefore, the contribution to the energy balance is from the difference in enthalpy of the solvent in the solution state and in the gas mixture.

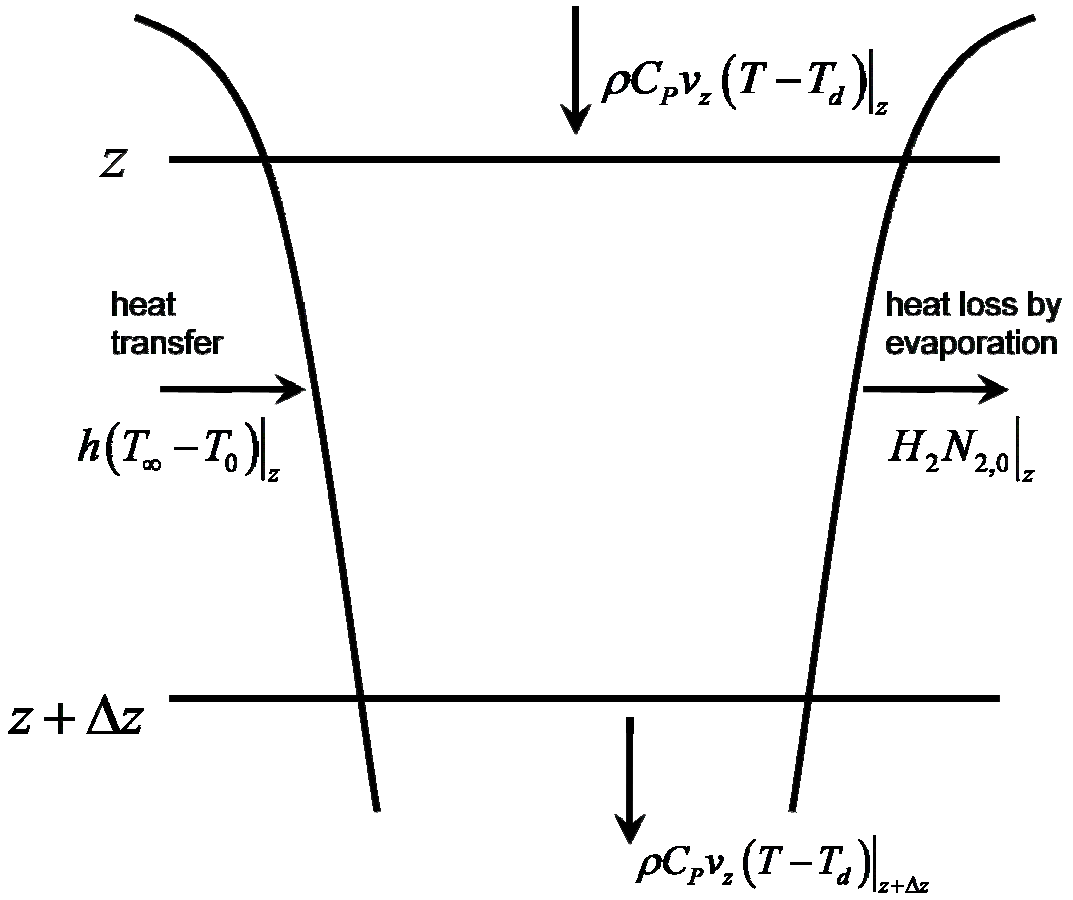

Figure 4.3 Differential volume element for the macroscopic energy balance.

The rate of the energy flow entering the z plane is:

$$\int_0^R 2\pi r \rho C_P v_z (T - T_d)\, dr$$

where, C_P is the specific heat and T_d is the datum, or reference temperature. The net convective energy flow into the DVE for small Δz is,

$$-\left\{\frac{\partial}{\partial z}\left[\int_0^R 2\pi r\rho C_P v_z\left(T-T_d\right)dr\right]\right\}\bullet\Delta z$$

Time rate of accumulation in the DVE is,

$$\left\{\frac{\partial}{\partial t}\left[\int_0^R 2\pi r\rho C_P\left(T-T_d\right)dr\right]\right\}\bullet\Delta z$$

Energy loss due to evaporation of the solvent across the filament/air interface is,

$$H_2 N_{2.0}\bullet 2\pi R\Delta z$$

where, H_2 is the partial molar enthalpy of the solvent on the gas-side with respect to T_d.

$$h\left(T_\infty - T_0\right)\bullet 2\pi R\Delta z$$

h is the heat transfer coefficient.

By assembling the above terms together and dividing the energy balance by Δz, the macroscopic energy equation is determined after taking the Δz limit to zero:

$$\frac{\partial}{\partial t}\left[\int_0^R 2\pi r\rho C_P\left(T-T_d\right)dr\right]=-\frac{\partial}{\partial z}\left[\int_0^R 2\pi r\rho C_P v_z\left(T-T_d\right)dr\right] -2\pi RH_2N_{2.0}+2\pi Rh\left(T_\infty-T_0\right) \tag{4.19}$$

After taking the integrals and simplifying:

$$\frac{\partial}{\partial t}\left[\frac{C_P W}{v_z}\left(T-T_d\right)\right]+\left[\frac{\partial}{\partial z}\left[C_P W\left(T-T_d\right)\right]\right] +2\pi R H_2 N_{2.0}-2\pi R\left(T_\infty-T_0\right)=0 \tag{4.20}$$

Then it is differentiated:

$$\frac{C_P W}{v_z}\left(\frac{\partial T}{\partial t}+v_z\frac{\partial T}{\partial z}\right)=2\pi Rh\left(T_\infty-T_0\right)-2\pi R H_2 N_{2.0}- C_P\left(T-T_d\right)\left[\frac{\partial}{\partial t}\left(\frac{W}{v_z}\right)+\frac{\partial W}{\partial z}\right] \tag{4.21}$$

Substituting equation (4.15) into the third term of equation (4.21) yields,

Assumption 5: The difference between the enthalpy of the solvent on the filament-side and that on the gas-side is approximated by the latent heat of vaporization of the solvent, ΔH_{vap} at the boiling point.

$$\frac{C_P W}{v_z}\left(\frac{\partial T}{\partial t}+v_z\frac{\partial T}{\partial z}\right)=2\pi Rh\left(T_\infty-T_0\right)-2\pi R N_{2,0}\left[H_2-M_2 C_P\left(T-T_d\right)\right] \tag{4.22}$$

$$\rho C_P\left(\frac{\partial T}{\partial t}+v_z\frac{\partial T}{\partial z}\right)=2\sqrt{\frac{\pi}{A}}\left[h\left(T_\infty-T_0\right)-\Delta H_{vap}N_{2,0}\right] \tag{4.23}$$

At steady-state, the time derivatives become zero and equation (4.23) becomes

$$\rho C_P v_z\frac{dT}{dx}=2\sqrt{\frac{\pi}{A}}\left[h\left(T_\infty-T_0\right)-\Delta H_{vap}N_{2,0}\right] \tag{4.24}$$

By substituting equations (4.1) and (4.18), the ordinary differential equation for the temperature of the filament is derived:

$$\frac{dT}{dx} = \frac{1}{C_P}\left[\frac{1-\omega_2}{W_1} \bullet 2h\sqrt{\pi A}\left(T_\infty - T_0\right) + \frac{\Delta H_{vap}}{M_2\left(1-\omega_2\right)} \bullet \frac{d\omega_2}{dz}\right] \tag{4.25}$$

4.4 Momentum Balance Equation

The overall momentum balance in the z direction follows the form,

$$\begin{Bmatrix}\text{rate of momentum}\\ \text{accumulation}\end{Bmatrix} = \begin{Bmatrix}\text{net momentum flow}\\ \text{into the DVE}\end{Bmatrix} + \begin{Bmatrix}\text{sum of the forces}\\ \text{acting on the system}\end{Bmatrix} \tag{4.26}$$

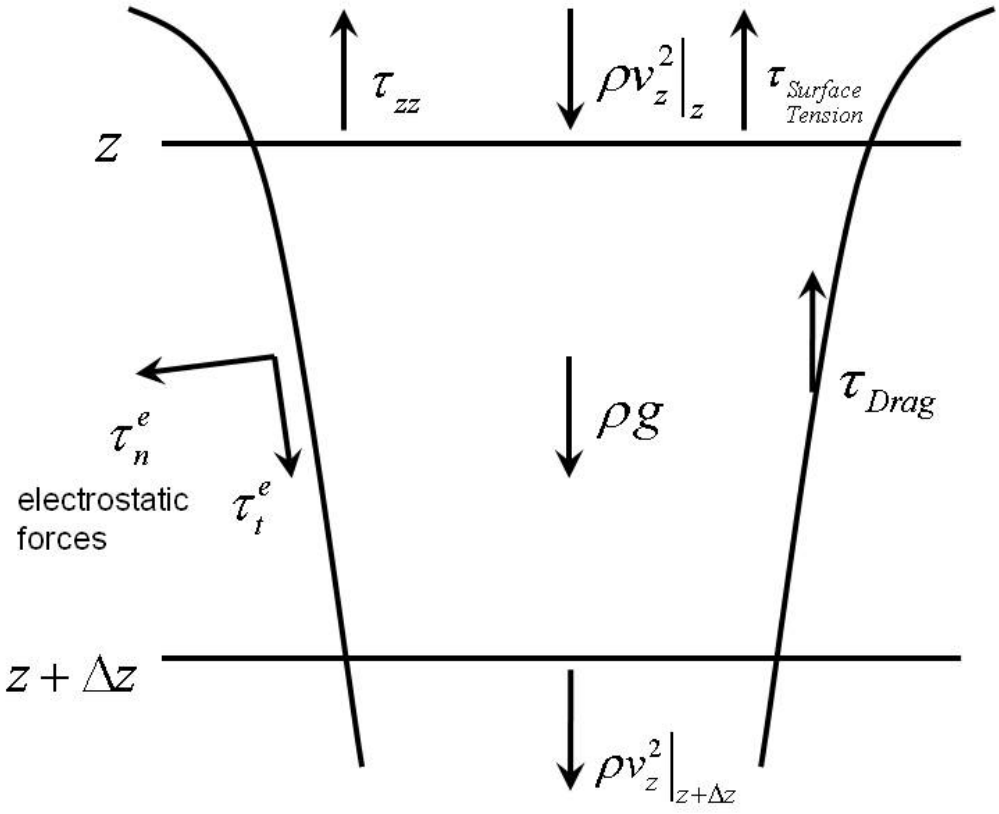

Figure 4.4 Differential volume element for the macroscopic momentum balance

The convective momentum rate entering the DVE at z is,

$$\int_0^R 2\pi r \rho v_z v_z dr$$

The net convective momentum flow for small Δz is,

$$\int_0^R 2\pi r \rho v_z^2 dr\Big|_{z=z} - \int_0^R 2\pi r \rho v_z^2 dr\Big|_{z=z+\Delta z} = -\left[\frac{\partial}{\partial z}\left(\int_0^R 2\pi r \rho v_z^2 dr\right)\right]\bullet\Delta z$$

The rheological force due to the polymer solution viscosity is,

$$F = \int_0^R 2\pi r \tau_{zz} dr$$

In addition to the convective momentum flow and the rheological force, there are the external forces acting on the system. These forces are due to gravity, air drag, surface tension, and the electrohydrodynamic stresses. With the downward direction of the filament representing the positive direction, the components of macroscopic equation of motion are shown (refer to Figure 4.4):

Time rate of momentum accumulation in the DVE:

$$\left[\frac{\partial}{\partial t}\left(\int_0^R 2\pi r \rho v_z dr\right)\right]\bullet\Delta z$$

Net convective momentum flow into the DVE, i.e., the inertial term:

$$-\left[\frac{\partial}{\partial z}\left(\int_0^R 2\pi r\rho v_z{}^2 dr\right)\right]\bullet\Delta z$$

Rheological force is:

$$-\left[\frac{\partial}{\partial z}\left(\int_0^R 2\pi r\tau_{zz} dr\right)\right]\bullet\Delta z$$

Gravitational force is given by

$$\left[\int_0^R 2\pi r\rho g dr\right]\bullet\Delta z$$

The air drag force is:

$$-\tau_{drag}\bullet 2\pi R\Delta z$$

The surface tension force is:

$$-\frac{\partial}{\partial z}(\gamma 2\pi r)$$

The electrostatic force is:

$$2\pi R\left(t_t^e - t_n^e\frac{dr}{dz}\right)$$

When these components are substituted back into the form of equation (4.26) and dividing the resulting equation by Δz and taking the limit as Δz approaches zero, the macroscopic equation of motion is obtained:

$$\frac{\partial}{\partial t}\left(\int_0^R 2\pi r\rho v_z dr\right) = -\frac{\partial}{\partial z}\left(\int_0^R 2\pi r\rho v_z{}^2 dr\right) + \frac{\partial}{\partial z}\left(\int_0^R 2\pi r\tau_{zz} dr\right) + \int_0^R 2\pi r\rho g dr \\ -\tau_{drag}\bullet 2\pi R - \frac{\partial}{\partial z}\left(\gamma 2\pi r\right) + 2\pi R\left(t_t^e - t_n^e \frac{dr}{dz}\right) \tag{4.27}$$

At steady state, the time derivative term becomes zero and performing the integration yields:

$$\frac{d}{dz}\left(\pi R^2\rho v_z{}^2\right) = \frac{d}{dz}\left(\pi R^2\tau_{zz}\right) + \frac{d}{dz}\left(\pi R^2\rho g\right) - \tau_{drag}\bullet 2\pi R - \frac{d}{dz}\left(\gamma 2\pi R\right) + 2\pi R\left(t_t^e - t_n^e \frac{dR}{dz}\right) \tag{4.28}$$

The rheological force is given by the normal stress difference:

$$\tau_{zz} - \tau_{rr} = 3\eta_0 \frac{dv}{dz}$$

The Trouton viscosity, i.e., the Newtonian elongational viscosity, is three times the zero-shear viscosity. The normal stress, τ_{rr}, is taken as zero because velocity in the radial direction is assumed to be constant.

4.5 The Axial Electric Field Equation

The axial electric field within the filament is derived from Coulomb's law for the potential along the center line of the jet:[23]

$$\psi(z) = \psi_{\infty}(z) + \frac{1}{2\bar{\varepsilon}} \int \frac{\sigma R d\zeta}{\sqrt{(z-\zeta)^2 + R^2}} - \frac{\beta}{4} \int \frac{d\left(ER^2\right)/d\zeta}{\sqrt{(z-\zeta)^2 + R^2}} d\zeta$$

The axial field is then given by,

$$E(z) = E_{\infty}(z) - \ln \chi \left(\frac{1}{\bar{\varepsilon}} \frac{d(\sigma R)}{dz} - \frac{\beta}{2} \frac{d^2\left(ER^2\right)}{dz^2} \right) \tag{4.29}$$

In addition to the electric field equation, the value for the surface charge density is required for calculating the electrostatic forces. It is derived from the conservation of charge equation, where the first term is for the charge traveling inside the filament and the second term is for the charge traveling on the outside surface of the filament:

$$\pi R^2 KE + 2\pi R v \sigma = I \tag{4.30}$$

The final first-order ordinary differential equations used in the model are:

$$\frac{d\omega_s}{dz} = \frac{-2\sqrt{\pi A}}{W_p} M_s N_{s,0} \left(1-\omega_s\right)^2$$

$$\frac{dT}{dz} = \frac{1}{C_p} \left[\frac{1-\omega_s}{W_p} 2h\sqrt{\pi A}\left(T_a - T\right) + \frac{\Delta H_{vap}}{M_s\left(1-\omega_s\right)} \frac{d\omega_s}{dz} \right]$$

$$\frac{dV}{dz}=\left(2AV+3A'\eta_o+3A\eta_o{}'\right)^{-1}\left[\begin{array}{r}-\rho_f A'V^2-3A\eta_o\frac{d^2V}{dz^2}+A\rho_f g-\gamma 2\pi R'-C_f\pi R\rho_a\left(V_z-V_a\right)^2\\ +2\pi R\sigma E_z-\frac{\pi\sigma^2}{\bar{\varepsilon}}R'-\pi\left(\bar{\varepsilon}-\varepsilon\right)E_z{}^2RR'\end{array}\right]$$

$$\frac{dE}{dz}=\frac{R}{4}\left(\frac{dR}{dz}\right)^{-1}\left[\frac{2}{R^2\beta}\left[\frac{E_Z-E_{\infty(z)}}{\ln\chi}+\frac{1}{\bar{\varepsilon}}\frac{d\left(\sigma R\right)}{dz}\right]-\frac{d^2E}{dz^2}-\frac{2E}{R^2}\left(\frac{dR}{dz}\right)^2-\frac{2E}{R}\frac{d^2R}{dz^2}\right]$$

4.6 The Material Properties

The molar flux of the solvent is given by [18]

$$N_{1,0}=\frac{Ky\left(j_{2,0}-j_{2,\infty}\right)}{\left(1-j_{2,0}\right)}$$

The mole fraction of the solvent is given by [18]

$$j_2=p_2^{sat}\omega_2 e^{(1-\omega_2)}$$

The heat transfer coefficient is derived as a function of the Nusselt number:

$$h=\frac{k_a}{2R}Nu$$

The Nusselt number for parallel air flow is:[18]

$$Nu = 0.35 + 0.146\left[Re_p + \left(1.03 Re_w^{0.36} - 0.685\right)^2 \right]^{0.5}$$

The Reynolds numbers for the velocities of the filament and the air are respectively:

$$Re_w = 2Rv_z \frac{\rho_a}{\eta_a}$$

$$Re_p = 2Rv_a \frac{\rho_a}{\eta_a}$$

The mass transfer coefficient is given by the analogy with the heat transfer coefficient:[18]

$$\frac{h}{ky} = 4.86 \times 10^8$$

The air properties are shown below:[19]

$$\rho_a = \frac{0.351}{T_f}$$

$$T_f = \frac{T + T_a}{2}$$

$$\eta_a = \frac{\left(1.446 \times 10^{-5}\right) T_f^{1.5}}{\left(T_f + 113.9\right)}$$

$$k_a = \left[\left(4.49 \times 10^{-7}\right) T_f^{0.866}\right]\left(4.1868 \times 10^7\right)$$

The heat capacity of the filament is given by [19]

$$C_P = \phi_1 C_{P,1} + \phi_2 C_{P,2}$$

The volume fraction can be determined mass fraction and the density of the components:

$$\phi_2 = \frac{\omega_2}{\omega_2 + \left(\frac{\rho_2^0 \omega_2}{\rho_1^0} \right)}$$

The latent heat of vaporization :[39]

$$\Delta H_{vap} = \left[46.95 \exp\left(-0.2826 T_r\right) \left(1 - T_r\right)^{0.2826} \right] \times 10^{10}$$

with reduced temperature as:

$$T_r = \frac{T}{T_c}$$

The air drag coefficient is given by [40]

$$C_f = 0.77 Re^{-0.61}$$

$$Re = \frac{2R\rho\left(v_z - v_a\right)}{\eta_a}$$

The glass transition temperature for a binary polymer solution is given by the Kelley-Bueche equation:[41]

$$T_g = \frac{b\phi_2 T_{g,2} + \phi_1 T_{g,1}}{b\phi_2 + \phi_1}$$

The zero-shear viscosity of the polymer solution is calculated depending on the temperature value of the filament with respect to its T_g.[42, 43]

When the filament temperature is very high relative to its T_g:

$$\log \eta_{0,T} = \log \eta_{0,1.2T_g} + a\left(\frac{T_g}{T} - 1\right)$$

where

$$a = \frac{\Delta E}{2.3 R_g T_g}$$

$$\log \eta_{0,1.2T_g} = \Delta E\left[\frac{0.052 - \left(8.5\times10^{-5}\right)T_g}{T_g}\right] - 1.4 + a\left(\frac{T_g}{T} - 1\right)$$

When the filament temperature is near its T_g:

$$\log \eta_{0,T} = \Delta E\left[\frac{0.052 - \left(8.5\times10^{-5}\right)T_g}{T_g}\right] - 1.4 + \upsilon + 3.4\log\left(M_1 / M_{cr}\right)$$

where

$$\upsilon = \log\left(10^{\upsilon 1} + 10^{\upsilon 2} + 10^{\upsilon 3}\right)$$

$$\upsilon 1 = a\left(T_g / T - 1\right)$$

$$\upsilon 2 = 33\left(T_g / T\right) - 27.8$$

$$\upsilon 3 = \frac{8\left(T_g / T\right) - 6.5 - 0.01a}{0.6 - 0.02a}$$

The viscosity of the polymer solution, as function of the component viscosities, is then given by:

$$\log \eta_0 = \log \eta_{0,T} + \log\left(1 - \phi_2\right)$$

4.7 Results of the Model Test

Initial computer simulations generated data that was inconclusive and was determined to be due in part to the complexity of the modeled system and the subsequent computational difficulties encountered. The results show values which indicate that the mathematical solution failed to converge properly. Upon further investigation, it was found that the problems arose from the sections of the model responsible for calculating the polymer solution viscosity and the electrostatic forces. The extreme changes these quantities undergo within a small length of space, particularly in the initial region just beyond the jet origin, may be a factor in contributing to the numerical instability of the model. In addition to reevaluating the formulation of certain properties such as viscosity and the electrostatic tractions involved in elongating the filament, further tests have to be done to the program to develop a more robust and appropriate computational scheme.

CHAPTER 5

CONCLUSIONS

Although creating electrospun fibers is a fairly simple procedure, one must appreciate that the process of electrospinning is very complex and still not completely understood. However, careful attention to the parameters that affect electrospun fiber formation will increase the probability of attaining fibers of desired size, morphology, and uniformity. A novel electrospinning model has been created, incorporating principles of the dry spinning process and electrohydrodynamics. A theoretical framework has been established, from which a foundation for a deeper understanding of the complexities of the electrospinning process can be gained. The novel incorporation of the principles of electrohydrodynamics (as a mechanism for fluid movement) coupled with very high solvent evaporation rate characteristics contributed to a new and representative description of the extreme case of filament diameter reduction inherent in the electrospinning process.

APPENDIX

FORTRAN SOURCE CODE

A print out of the source code for the electrospinning model is presented. The "Main" program is shown below.

```
c                File: PhD ESPIN Imura  (Main program)
c                3/30/12
c

      program chao1
      implicit real*8 (a-h,o-z)
      include 'common'
      integer time
      external time
      dimension ycurrent(10),ylast(10)
            open(10,file='inputdat',status='old')
      open(20,file='output.m',status='unknown')
      write(*,200)
            pi=4.0d0*atan(1.0d0)
 200  format(1x,'Input iflag'/)
      read(10,*) iflag,ndim
      write(*,210)
 210  format(1x,'Input nfun')
      read(10,*) nfun
      write(*,220)
 220  format(1x,'Input yinit dt tmax')
      read(10,*) dt,tmax
      do 21 i=1,ndim
      read(10,*) yinit(i)
 21   continue
            xmf2=yinit(1)
            xmf1=1.0d0-xmf2
            vz=yinit(2)
            xt=yinit(4)
            e=yinit(5)
            xden1=1.31d0
            xden2=0.790d0
            xdenf=1.0d0
            xmw2=58.08d0
            xtg1=468.0d0
            xtg2=44.0d0
            xq=8.5d-4
            xg=980.7d0
            xst=39.0d0
            xw1=xmf1*xdenf*xq
            xr=dsqrt(xw1/(xdenf*xmf1*pi*vz))
            read(10,*) nwt
```

```
      nts=nint(tmax/dt)
      write(20,100) 1,0.0d0
      write(20,111) 1,yinit(1)
      write(20,112) 1,yinit(2)
      write(20,113) 1,yinit(3)
      write(20,114) 1,yinit(4)
      write(20,117) 1,yinit(5)
      write(20,118) 1,yinit(6)
            xrg=8.314472d7
            xdiea=0.0796d0
            xdief=1.4d0
            xva=0.0d0
            xta=300.0d0
            xae=47.5d0
            xb=(xdief/xdiea)-1.0d0
            xl=20.0d0
            xchi=xl/xr
            xelcd=1.5d5
            xcur=8994.0d0
            sigmac=(xcur/pi-e*(xr**2)*xelcd)/(2.0d0*xr*vz)
            xappvjc=2.0d4
            xappv=xappvjc*(299.8d0**-1.0d0)
            xeext=xappv/xl
            phi2=xmf2/(xmf2+(xden2*(xmf1)/xden1))
            phi1=1.0d0-phi2
            xxr=2.5d0
            xtg=(xxr*phi2*xtg2+phi1*xtg1)
     $                              /(xxr*phi2+phi1)
            write(20,115) 1,xr
            write(20,119) 1,xq
            write(20,120) 1,xcur
            write(20,121) 1,sigmac
            write(20,122) 1,xtg
      it=0
      do 23 i=1,ndim
        ylast(i)=yinit(i)
23    continue
      nc=0
      ni=1
      tlast=0.0d0
300   if (tlast+dt .le. tmax+2.0d-15) then
                        write(*,*) nc
        nc=nc+1
        it=it+1
        if (iflag .eq. 10) then
          call rk2(tlast,ylast,ycurrent)
        endif
        if (iflag .eq. 11) then
          call euler(tlast,ylast,ycurrent)
        endif
        if (iflag .eq. 9) then
          call rk4(tlast,ylast,ycurrent)
        endif
        if (mod(nc,nwt) .eq. 0) then
          ni=ni+1
          write(20,100) ni,tlast+dt*nwt
```

```
          write(20,111) ni,ycurrent(1)
          write(20,112) ni,ycurrent(2)
          write(20,113) ni,ycurrent(3)
          write(20,114) ni,ycurrent(4)
          write(20,117) ni,ycurrent(5)
          write(20,118) ni,ycurrent(6)

c                    ****10.0d4 is micron/cm convert for radius in microns

                     xr=10.0d4*dsqrt(xw1/(xdenf*(1.0d0-ycurrent(1))*pi*ycurrent(2)))
                     write(20,115) ni,xr
                     xsig=xcur/(2.0d0*pi*xr*ycurrent(2))-xr*xelcd*ycurrent(5)
     $                       /2.0d0/ycurrent(2)
                     xqcheck=(1.0d0-ycurrent(1))*pi*(xr**2)*ycurrent(2)
                     xicheck=pi*(xr**2)*xelcd*ycurrent(5)+
     $                       2.0d0*pi*xr*ycurrent(2)*xsig
                     phi2=ycurrent(1)/(ycurrent(1)+(xden2*(1.0d0-ycurrent(1))/xden1))
                     phi1=1.0d0-phi2
                     xtgcheck=(xxr*phi2*xtg2+phi1*xtg1)
     $                       /(xxr*phi2+phi1)
          write(20,119) ni,xqcheck
          write(20,120) ni,xicheck
          write(20,121) ni,xsig
                     write(20,122) ni,xtgcheck
               write(20,123) ni,xdenf
        endif
        tlast=tlast+dt
        do 25 i=1,ndim
          ylast(i)=ycurrent(i)
 25     continue
        go to 300
      endif
 100  format('z(',i10,')=',e26.16,';')
 111  format('mf2(',i10,')=',e26.16,';')
 112  format('vz(',i10,')=',e26.16,';')
 113  format('dvz(',i10,')=',e26.16,';')
 114  format('T(',i10,')=',e26.16,';')
 115  format('R(',i10,')=',e26.16,';')
 117  format('E(',i10,')=',e26.16,';')
 118  format('dEz(',i10,')=',e26.16,';')
 119  format('q(',i10,')=',e26.16,';')
 120  format('i(',i10,')=',e26.16,';')
 121  format('sig(',i10,')=',e26.16,';')
 122  format('Tg(',i10,')=',e26.16,';')
 123  format('denf(',i10,')=',e26.16,';')

      stop
      end
```

The subroutine: “Func” is shown below:

```
c                   PhD ESPIN Imura  (Subroutine-FUNC)
c                   3/30/12
c
c***********************************************

      subroutine func(yvalout,tin,yvalin)
      implicit real*8 (a-h,o-z)
      include 'common'
      dimension yvalout(10),yvalin(10)
            pi=4.0d0*atan(1.0d0)

            xmf2=yvalin(1)
            xmf1=1.0d0-xmf2
            vz=yvalin(2)
            dvz=yvalin(3)
            xt=yvalin(4)
            e=yvalin(5)
            de=yvalin(6)

      if (nfun .eq. 11) then
                  xcp1=1.32d7
                  xcp2=2.16d7
                  xtc=508.1d0
                  xtr=xt/xtc
                  xxr=2.5d0
                  phi2=xmf2/(xmf2+(xden2*xmf1)/xden1)
                  phi1=1.0d0-phi2
                  xtg=(xxr*phi2*xtg2+phi1*xtg1)
     $                  /(xxr*phi2+phi1)

                  xts=1.2d0*xtg
                  xdenf=1.0d0
                  xr=dsqrt(xw1/(xdenf*xmf1*pi*vz))
                  xa=pi*(xr**2.0d0)
                  xp2s=(10.0d0**(4.2184d0-(1197.01d0/(xt-45.09d0))))*1.0d6
                  xcp=phi1*xcp1+phi2*xcp2
                  xtf=0.5d0*xta+0.5d0*xt
                  xka=((4.49d-7)*(xtf**0.866d0))*(4.1868d7)
                  xdena=0.351d0/xtf
                  xvisca=((1.446d-5)*(xtf**1.5d0))/(xtf+113.9d0)
                  xhvap=(46.95d0*(dexp(-0.2826d0*xtr))*
     $                  ((1.0d0-xtr)**0.2826d0))*1.0d10
c           *********** fiber viscosity ***********
                  xtem=xae/(2.3d0*xrg*xt)
                  if (xt .gt. xts) then
                        xlgviscts=xae*((0.052d0-(8.5d-5)*xtg)/xtg)
     $                              -1.4d0+xtem*(xtg/xt-1.0d0)
                        xlgvisct=xlgviscts+xtem*(xtg/xt-1.0d0)
                  endif

                  if (xt .le. xts) then
                        xvk1=xtem*(xtg/xt-1.0d0)
                        xvk2=33.0d0*(xtg/xt)-27.8d0
```

```
                        xvk3=(8.0d0*(xtg/xt)-6.5d0-0.01d0*xtem)
     $                        /(0.6d0-0.02d0*xtem)
                        xvk=log10((10.0**xvk1)+(10.0d0**xvk2)
     $                        +(10.0d0**xvk3))
                        xlgvisct=xae*((0.052d0-(8.5d-5)*xtg)/xtg)
     $                        +1.6056d0+xvk
                  endif
c        ***************** filament viscosity*****
                  xviscf=(10.0d0**(xlgvisct+5.0d0*log10(phi1)))*10.0d0
                  xrew=2.0d0*xr*vz*xdena/xvisca
c        ****** heat transfer coeff. (parallel case)*****
                  xrep=2.0d0*xr*xva*xdena/xvisca
                  xnu=0.35d0+0.146d0*dsqrt(xrep+(1.03d0*(xrew
     $                  **0.36d0)-0.685d0)**2.0d0)
                  xh=xka*xnu/2.0d0*xr
                  xky=xh/(4.86d8)
                  xj2=xp2s*xmf2*dexp(xmf1)
                  xj2a=0.0d0
                  xnx2=xky*(xj2-xj2a)/(1.0d0-xj2)
                  yvalout(1)=-2.0d0*(dsqrt(pi*xa))
     $                        *xmw2*xnx2*(xmf1**2.0d0)/xw1
                  yvalout(2)=dvz
                  yvalout(4)=((xmf1/xw1)*2.0d0*xh*(dsqrt(pi*xa))
     $                        *(xta-xt)+(xhvap/(xmw2*xmf1))
     $                        *yvalout(1))/xcp
                  xdr=0.5d0*(dsqrt(xw1/(pi*xdenf*xmf1*vz)))
     $                  *((yvalout(1)/xmf1)-(dvz/vz))
                  xtf=xt/2.0d0+xta/2.0d0
                  xdtf=0.5d0*yvalout(4)
                  xdka=16.2797d0*(xtf**-0.134d0)*xdtf
                  xddena=-0.351d0*(xtf**-2.0d0)*xdtf
c                 **** derivative of Nusselt number ****

                  xrewu=2.0d0*xr*vz*xdena
                  xrewv=xvisca
                  xrewdu=2.0d0*(xdr*vz*xdena+xr*xdena*dvz
     $                  +xr*vz*xddena)
                  xdvisca=1.446d-5*(1.5d0*(dsqrt(xtf))*xdtf
     $                        /(xtf+113.9d0)-(xtf**1.5d0)
     $                        *((xtf+113.9d0)**-2.0d0)*xdtf)
                  xrewdv=xdvisca
                  xdrew=(xrewdu*xrewv-xrewu*xrewdv)/(xrewv**2.0d0)
                  xrepu=2.0d0*xr*xva*xdena
                  xrepv=xvisca
                  xrepdu=2.0d0*(xdr*xva*xdena+xr*xva*xddena)
                  xrepdv=xdvisca
                  xdrep=(xrepdu*xrepv-xrepu*xrepdv)/(xrepv**2.0d0)
                  xdnu=0.073d0/dsqrt(xrep+(1.03d0*(xrew**0.36d0)
     $                  -0.685d0)**2.0d0)
     $                  *(xdrep+2.0d0*(1.03d0*(xrew**0.36d0)
     $                  -0.685d0)*(0.3708d0*(xrew**-0.64d0)*xdrew))
                  xdh=-2.0d0*xdr*xka*xdnu/(xr**2.0d0)
     $                  +xdka/(2.0d0*xr)+xka*xdnu/(2.0d0*xr)
                  xdky=xdh/(4.86d8)
                  xdp2s=1.0d6*((10.0d0**(4.2184d0-
     $                  (1197.01d0/(xt-45.09d0))))*(dlog(10.0d0)))
```

```
                xdj2=xdp2s*xmf2*(dexp(xmf1))
     $                  +xp2s*yvalout(1)*(dexp(xmf1))
     $                  +xp2s*xmf1*(dexp(xmf1))*(-yvalout(1))
                xtem=1.0d0-xj2
                xdnx2=xdky*xj2/xtem+xky*xdj2/xtem
     $                  +xky*xj2*(xdj2/(xtem**2.0d0))
                xda=2.0d0*pi*xr*xdr
c       ******** double deriv. of mass frac. solvent********
                x2dmf2=(-2.0d0*xmw2/xw1)*((0.5d0/dsqrt(pi*xa))
     $                  *pi*xda*xnx2*(xmf1**2.0d0)
     $                  +(dsqrt(pi*xa))*xdnx2*(xmf1**2.0d0)
     $                  +(dsqrt(pi*xa))*xnx2*2.0d0*xmf1
     $                  *(-yvalout(1)))
c       ********* double deriv. of r **********************
                xaa=xr/2.0d0
                xdnn=(xmf1**-1.0d0)*(-vz**-2.0d0)*dvz
     $                  +((xmf1**-2.0d0)*yvalout(1)/vz)
                xdaa=0.25d0*(1.0d0/xr)*(xw1*xdnn/pi/xdenf)
                xbb=yvalout(1)/xmf1-dvz/vz
                xdbb1=x2dmf2/xmf1+(yvalout(1)
     $                  /(xmf1**2.0d0))*yvalout(1)
                xdbb2=yvalout(3)/vz+(-vz**-2.0d0)*(dvz**2.0d0)
                xdbb=xdbb1-xdbb2
                x2dr=xaa*xdbb+xdaa*xbb
c       *********electrical equations**********************
                xdsig=xdr*(-xelcd/vz-1.0d0/(xr*vz))
     $                  -(xelcd*xr/2.0d0/vz)*de
     $                  -(dvz/vz)
                xsig=xcur/(2.0d0*pi*xr*vz)-xr*xelcd*e/2.0d0/vz
                xdsigr=xr*xdsig+xsig*xdr
                yvalout(6)=(2.0d0/(xr**2.0d0)/xb)
     $                  *((e-xeext)/dlog(xchi)+xdsigr
     $                  /xdiea)-4.0d0*de*xdr/xr
     $                  -2.0d0*e/(xr**2.0d0)*(xdr**2.0d0)
     $                  -2.0d0*e/xr*x2dr
c       ******** drag coeff.:vibrating air  **************
                xre=2.0d0*xr*xdena*(vz-xva)/xdena
                xcf=0.77d0*(xre**-0.61d0)
                xdviscf=((10.0d0**(xlgvisct+5.0d0*(log10(phi1)))
     $                  )*dlog(10.0d0))*10.0d0
                yvalout(3)=(-xdenf*xda*(vz**2.0d0)
     $                  -dvz*(2.0d0*xa*vz+3.0d0*xda
     $                  *xviscf+3.0d0*xda*xdviscf)
     $                  +xa*xdenf*xg-xst*2.0d0*pi*xdr
     $                  -xcf*pi*xr*xdena*((vz-xva)**2.0d0)
     $                  +2.0d0*pi*xr*xsig*e
     $                -pi*(xsig**2.0d0)*xdr/xdiea
     $                  -pi*(xdiea-xdief)*(e**2.0d0)
     $                  *xr*xdr)/(3.0d0*xa*xviscf)
c       write(*,*) xvism,xdvism
        write(*,*) yvalout(1),yvalout(2),yvalout(3)
        write(*,*) yvalout(4),yvalout(5),yvalout(6)
        endif
    return
    end
```

The subroutine “RK4” (Runge-Kutta 4th order) is shown below:

```
c          Subroutine rk4 (Runge-Kutta 4th order)

           subroutine rk4(tlast,ylast,ycurrent)
           implicit real*8 (a-h,o-z)
      include 'common'
           dimension ycurrent(10),ylast(10),yvalin(10)
      dimension tem1(10),tem2(10),tem3(10),tem4(10)
      call func(tem1,tlast,ylast)
           do 10 i=1,ndim
      yvalin(i)=ylast(i)+dt*tem1(i)/2.0d0
 10   continue
           tin=tlast+dt/2.0d0
      call func(tem2,tin,yvalin)
      yvalin(i)=ylast(i)+dt*tem2(i)/2.0d0
      tin=tlast+dt/2.0d0
      call func(tem3,tin,yvalin)
      yvalin(i)=ylast(i)+dt*tem3(i)
      tin=tlast+dt
      call func(tem4,tin,yvalin)
      ycurrent(i)=ylast(i)+dt*(tem1(i)+2.0d0*tem2(i)
     $ +2.0d0*tem3(i)+tem4(i))/6.0d0
      return
      end
```

REFERENCES

1. Y. Filatov, A. Budyka and V. Kirichenko, *Electrospinning of micro- and nanofibers: fundamentals and applications in separation and filtrattion processes*. (Begell House, Redding, CT, USA, 2007).

2. S. Shanmugasundaram, Y. Imura, T. Arinzeh and M. Jaffe, in *Tissue Engineering: Roles, Materials and Applications*, edited by S. Barnes and L. Harris (Nova Publishers, Hauppauge, USA, 2008), pp. 83-97.

3. M. Li, M. J. Mondrinos, M. R. Gandhi, F. K. Ko, A. S. Weiss and P. I. Lelkes, Biomaterials **26** (30), 5999-6008 (2005).

4. S. Y. Chew, Y. Wen, Y. Dzenis and K. W. Leong, Current Pharmaceutical Design **12** (36), 4751-4770 (2006).

5. J. Zeleny, Physical Review **10** (1), 1-6 (1917).

6. A. Formhals, US Patent No. 1,975,504 (1934).

7. M. Cloupeau and B. Prunet-Foch, Journal of Aerosol Science **25** (6), 1021-1036 (1994).

8. D. R. Salem, *Structure Formation in Polymeric Fibers*. (Hanser Verlag, 2001).

9. G. I. Taylor, Proc. R. Soc. London, Ser. A **280**, 383-397 (1964).

10. G. I. Taylor, Proc. R. Soc. London, Ser. A **313**, 453-475 (1969).

11. I. Marginean, L. Parvin, L. Heffernan and A. Vertes, Analytical Chemistry **76** (14), 4202-4207 (2004).

12. Y. M. Shin, M. M. Hohman, M. P. Brenner and G. C. Rutledge, Applied Physics Letters **78** (8), 1149-1151 (2001).

13. D. H. Reneker and A. L. Yarin, Polymer **49** (10), 2387-2425 (2008).

14. P. K. Baumgarten, J. Colloid Interface Sc. **36**, 71-29 (1971).

15. D. H. Reneker, A. L. Yarin, H. Fong and S. Koombhongse, Journal of Applied Physics **87** (9 I), 4531-4547 (2000).

16. F. J. Higuera, Physical Review E - Statistical, Nonlinear, and Soft Matter Physics **68** (1 2), 163041-1630410 (2003).

17. I. Brazinsky, A. G. Williams and H. L. Lanieve, Polym. Eng. Sci. **15**, 834-841 (1975).

18. Y. Ohzawa, Y. Nagano and T. Matsuo, J. Appl. Polym. Sci. **13** (2), 257-283 (1969).

19. Z. Gou and A. J. McHugh, Journal of Applied Polymer Science **87** (13), 2136-2145 (2003).

20. J. F. de la Mora, Annual Review of Fluid Mechanics **39**, 217-243 (2007).

21. A. F. Spivak and Y. A. Dzenis, Applied Physics Letters **73** (21), 3067-3069 (1998).

22. M. M. Hohman, M. Shin, G. Rutledge and M. P. Brenner, Physics of Fluids **13** (8), 2201-2220 (2001).

23. J. J. Feng, Physics of Fluids **14** (11), 3912-3926 (2002).

24. S. Tripatanasuwan, Z. Zhong and D. H. Reneker, Polymer **48** (19), 5742-5746 (2007).

25. G. Taylor, Proceedings of the Royal Society of London. Series A. Mathematical and Physical Sciences **291** (1425), 159-166 (1966).

26. D. A. Saville, Annual Review of Fluid Mechanics **29**, 27-64 (1997).

27. J. R. Melcher and G. I. Taylor, Annual Review of Fluid Mechanics **1**, 111-146 (1969).

28. J. Fernández de la Mora, (2007), Vol. 39, pp. 217-243.

29. A. M. Gañán-Calvo, J. Dávila and A. Barrero, Journal of Aerosol Science **28** (2), 249-275 (1997).

30. L. D. Landau, E. M. Lifshitz and L. P. Pitaevskii, *Electrodynamics of continuous media*, 2nd ed. (Butterworth-Heinemann, Oxford, 1984).

31. W. B. Russel, *Colloidal Dispersions*. (Cambridge University Press, New York, 1991).

32. S. Torza, R. G. Cox and S. G. Mason, Phil Trans Roy Soc London Ser A. Math Phys Sci **269** (1198), 295-310 (1971).

33. J. C. Baygents, Saville, D.A., presented at the Drops and Bubbles, Third International Colloquium, Monterey, 1988 (unpublished).

34. O. Vizika and D. A. Saville, Journal of Fluid Mechanics **239**, 1-21 (1992).

35. T. Tsukada, Katayama, T., Ito, Y., Hozawa, M., J. Chem. Eng. Jpn. **26**, 698-703 (1993).

36. A. J. Mestel, Journal of Fluid Mechanics **274**, 93-113 (1994).

37. F. J. Higuera, Journal of Fluid Mechanics **648**, 35-52 (2010).

38. G. Riboux, A. G. Marnín, I. G. Loscertales and A. Barrero, Journal of Fluid Mechanics **671**, 226-253 (2011).

39. V. Majer and V. Svoboda, *Enthalpies of Vaporization of Organic Compounds: A Critical Review and Data Compilation*. (Blackwell Scientific Publications, Oxford, 1985).

40. J. Shimizu, N. Okui and K. Tamai, Sen-I Gakkaishi **39**, 62 (1983).

41. F. N. Kelley and F. Bueche, J Polym Sci **50**, 549-556 (1961).

42. D. W. Van Krevelen and K. Te Nijenhuis, *Properties of Polymers*, 4 ed. (Elsevier B.V., Amsterdam, 2009).

43. Y. Sano, Drying Technology **19** (7), 1335-1359 (2001).